

1 **Toward Understanding the Simulated Phase Partitioning of Arctic Single-**
2 **Layer Mixed-Phase Clouds in E3SM**

3
4 Meng Zhang¹, Shaocheng Xie², Xiaohong Liu^{1*}, Wuyin Lin³, Kai Zhang⁴, Hsi-Yen Ma², Xue
5 Zheng², Yuying Zhang²

6
7 ¹ Department of Atmospheric Sciences, Texas A&M University, College Station, Texas, USA

8 ² Lawrence Livermore National Laboratory, Livermore, CA, USA,

9 ³ Brookhaven National Laboratory, Upton, NY, USA,

10 ⁴ Pacific Northwest National Laboratory, Richland, WA, USA

11
12 * Correspondence to X. Liu, xiaohong.liu@tamu.edu

13 **Key Points:**

- 14 • EAMv1 simulated Arctic single-layer mixed-phase clouds are overly dominated by
15 supercooled liquid with little ice produced;
- 16 • Insufficient heterogeneous ice nucleation by CNT at warm temperatures is responsible
17 for the underestimation of cloud ice formation;
- 18 • Lacking the ice phase processes in CLUBB and its interaction with stratiform cloud
19 microphysics limits the growth of cloud ice.

20 **Abstract**

21 Significant changes are found in the modeled phase partitioning of Arctic mixed-phase clouds in
22 the U.S. Department of Energy (DOE) Energy Exascale Earth System Model (E3SM)
23 Atmosphere Model version 1 (EAMv1) compared to its predecessor, the Community
24 Atmosphere Model version 5 (CAM5). In this study, we aim to understand how the changes in
25 modeled mixed-phase cloud properties are attributed to the updates made in the EAMv1 physical
26 parameterizations. Impacts of the Classical Nucleation Theory (CNT) ice nucleation scheme, the
27 Cloud Layer Unified By Binormals (CLUBB) parameterization, and updated Morrison and
28 Gettelman microphysical scheme (MG2) are examined. Sensitivity experiments using the short-
29 term hindcast approach are performed to isolate the impact of these new features on simulated
30 mixed-phase clouds. Results are compared to the DOE's Atmospheric Radiation Measurement
31 (ARM) Mixed-Phase Arctic Cloud Experiment (M-PACE) observations. We find that mixed-
32 phase clouds simulated in EAMv1 are overly dominated by supercooled liquid and cloud ice
33 water is substantially underestimated. The individual change of physical parameterizations is
34 found to decrease cloud ice water mass mixing ratio in EAMv1 simulated single-layer mixed-
35 phase clouds. A budget analysis of detailed cloud microphysical processes suggests that the lack
36 of ice particles that participate in the mass growth processes strongly inhibits the mass mixing
37 ratio of cloud ice. The insufficient heterogeneous ice nucleation at temperatures warmer than -
38 15°C in CNT and the negligible ice processes in CLUBB are primarily responsible for the
39 significant underestimation of cloud ice water content in the Arctic single-layer mixed-phase
40 clouds.

41

42 **1. Introduction**

43 Mixed-phase clouds, which are composed of both ice crystals and supercooled liquid
44 droplets, are found to have significant impacts on the sea ice and ice sheet melt (Bannartz et al.,
45 2013; Hofer et al., 2019; Nicolas et al., 2017) and regional and global climate change (Lawson &
46 Gettelman, 2014; Lohmann & Neubauer, 2018; Tan & Storelvmo, 2019). Observations show that
47 mixed-phase clouds occur with high spatial and temporal frequencies in the high latitudes (de
48 Boer et al., 2009; Zhang D. et al., 2018, 2019) and are observed most frequently during the
49 spring and fall seasons in the Arctic (Shupe et al., 2006, 2011). Because of the vastly different
50 optical properties between liquid droplets and ice crystals, cloud water phase partitioning
51 between liquid and ice in mixed-phase clouds can substantially impact the radiative fluxes at the
52 surface and alter the surface energy budget (Bannartz et al., 2013; Hofer et al., 2019; Nicolas et
53 al., 2017).

54 It is imperative for global climate models (GCMs) to capture the spatial distribution and
55 microphysical properties of mixed-phase clouds in order to achieve an accurate future climate
56 prediction. However, large uncertainties remain in the modeling of mixed-phase clouds in most
57 current GCMs (Barrett et al., 2017; Klein et al., 2009; Komurcu et al., 2014; Morrison et al.,
58 2009). For example, the temperature at which amounts of cloud liquid water and ice water are
59 equally abundant in simulated mixed-phase clouds over the Southern Ocean varies by 40°C
60 among 19 Coupled Model Intercomparison Project Phase 5 (CMIP5) models (McCoy et al., 2015,
61 2016). One of the challenges in modeling mixed-phase clouds lies in the representation of
62 heterogeneous ice nucleation that occurs at temperatures warmer than -37°C (Liu et al., 2011; Shi
63 & Liu, 2019; Xie et al., 2008, 2013). Different parameterizations for heterogeneous ice

64 nucleation derived from laboratory measurements (DeMott et al., 2015; Niemand et al., 2012),
65 field observations (DeMott et al., 2010) or based on the Classical Nucleation Theory (CNT)
66 (Hoose et al., 2010; Wang et al., 2014) are used in GCMs, which results in considerable
67 uncertainties in the simulated ice particle number concentration of mixed-phase clouds. Another
68 challenge exists in the treatment of ice depositional growth through the Wegner-Bergeron-
69 Findeisen (WBF) process in mixed-phase clouds. The WBF process controls the growth of ice
70 particles at the expense of coexisting liquid droplets because of the lower equilibrium vapor
71 pressure with respect to ice than that with respect to liquid at temperatures colder than 0°C. It is
72 found that simulated mixed-phase cloud phase partitioning is strongly sensitive to the treatment
73 of WBF process in GCMs. The representation of WBF process which ignores the subgrid cloud
74 structures generally leads to underestimation of liquid water mass mixing ratio (Storelvmo et al.,
75 2008; Tan & Storelvmo, 2016; Zhang M. et al., 2019). In addition, the interaction between cloud
76 microphysics and other physical processes, such as shallow convection, is also found to play an
77 important role in modeled mixed-phase cloud microphysical properties. For example, the
78 excessive surface shortwave radiative fluxes over the Southern Ocean are much reduced with an
79 enhanced amount of cloud liquid water in simulated mixed-phase clouds when more liquid is
80 allowed to be detrained from shallow convection into stratiform clouds in the Community
81 Atmosphere Model version 5 (CAM5) (Kay et al., 2016; Wang et al., 2018).

82 The treatment of stratiform and convective cloud processes in the U.S. Department of
83 Energy (DOE) state-of-the-art GCM, Energy Exascale Earth System Model (E3SM) atmosphere
84 model version 1 (EAMv1) (Golaz et al., 2019; Rasch et al., 2019; Xie et al., 2018), has been
85 developed in many ways from CAM5, which EAMv1 is built on. In terms of the cloud physical

86 parameterizations associated with mixed-phase clouds, first of all, EAMv1 adopts the CNT ice
87 nucleation scheme to represent immersion, contact, and deposition nucleation in mixed-phase
88 clouds (Wang et al., 2014). Compared to the previous temperature dependent heterogeneous ice
89 nucleation scheme (Meyers et al., 1992) in CAM5, simulated mixed-phase cloud supercooled
90 liquid fraction (SLF), which is defined as the ratio of liquid water mass to total condensed water
91 mass, is significantly increased at temperatures colder than -20°C over the polar areas with CNT.
92 Reduced ice nucleating particle (INP) number concentration with CNT is found to mostly
93 explain the increased SLF in modeled clouds (Wang et al., 2018). Second, the Cloud Layers
94 Unified By Binormals (CLUBB) parameterization is implemented in EAMv1 to treat planetary
95 boundary layer (PBL) turbulence, shallow convection, and cloud macrophysics in a unified
96 framework (Golaz et al., 2002; Larson, 2017; Larson & Golaz, 2005). Simulated marine
97 boundary layer clouds show significant improvements in terms of the vertical distribution of
98 cloud layers and the daily variability of cloud cover (Zheng et al., 2016). The transition from
99 stratocumulus to cumulus clouds is also better simulated by CLUBB (Bogenschutz et al., 2012,
100 2013). Moreover, EAMv1 uses the second version of two-moment cloud microphysical scheme
101 (Gettelman & Morrison, 2014) (MG2). The new scheme predicts the mass and number mixing
102 ratios of snow and rain hydrometeors instead of the diagnostic treatment in its earlier version
103 (MG1) (Morrison & Gettelman, 2008). The collection of liquid droplets by rain drops through
104 the accretion process tends to become more dominant than autoconversion, which is more
105 comparable to the idealized simulations (Gettelman et al., 2015). Finally, the WBF process with
106 respect to both ice and snow has been slowed down by 10 times in EAMv1 through a tuning
107 parameter. The growth rate of ice crystals at the expense of liquid droplets is then reduced by a

108 factor of 10 globally, regardless of the spatial distribution of mixed-phase clouds. This parameter
109 has been found to be over-tuned, particularly with the use of the new CNT ice nucleation scheme
110 in EAMv1 as we discuss later. This issue is being addressed by the E3SM development team.

111 With these new features and other improvements, EAMv1 shows promising
112 improvements in the simulated cloud climatology, cloud radiative effect, and global precipitation
113 (Xie et al., 2018). In contrast to CAM5, however, EAMv1 is found to have too large liquid phase
114 cloud fraction and a moderate underestimation of ice phase cloud fraction between -20°C and -
115 30°C temperature range over the high-latitudes in both hemispheres (Zhang Y. et al., 2019). The
116 simulated SLF of mixed-phase clouds is significantly larger than CAM5 for temperatures colder
117 than -13°C, and larger than observations for temperatures colder than -25°C. The increased
118 supercooled liquid in EAMv1 is partially related to the artificially reduced WBF process rate and
119 the use of CNT ice nucleation scheme as illustrated in Zhang Y. et al. (2019). They found that
120 SLF is significantly reduced by setting the tuning parameter back to 1. However, it is still much
121 larger than that produced by CAM5. This indicates that other changes in the model physics made
122 in EAMv1 also play an important role in increasing SLF in mixed-phase clouds from CAM5 to
123 EAMv1.

124 The goal of this study is to provide a process-level understanding on how the changes in
125 EAMv1 physical parameterizations impact the simulated single-layer mixed-phase clouds, with
126 an emphasis on the Arctic, beyond the impact from the artificial tuning parameter applied to the
127 WBF process. This is done through well-designed sensitivity experiments, which are conducted
128 by utilizing a short-term hindcast framework developed by the DOE Cloud-Associated
129 Parameterizations Testbed (CAPT) project (Ma et al., 2015; Phillips et al., 2004). Under the

130 CAPT framework, climate models can be initialized with reanalysis dataset and run in the short-
131 term hindcast mode. This allows a direct comparison between model simulations and observation
132 data collected in field campaigns, such as those conducted from the DOE Atmospheric Radiation
133 Measurement (ARM) program. Earlier studies indicate that most climate model errors in clouds
134 and precipitation, which are associated with fast physical processes, could appear in the day-2
135 hindcasts and the errors then gradually saturate (Ma et al., 2014; Xie et al., 2012). This approach
136 has been widely used to understand and improve cloud related parameterizations in climate
137 models (Liu et al., 2011; Xie et al., 2008; Zheng et al., 2016).

138 In this study, a series of short-term hindcasts with EAMv1 are conducted for the DOE
139 ARM Mixed-Phase Arctic Cloud Experiment (M-PACE) field campaign (Verlinde et al., 2007),
140 which was conducted at the ARM North Slope of Alaska (NSA) site during October 2004.
141 Hindcasts are initialized with the European Centre for Medium-Range Weather Forecasts
142 (ECMWF) ERA-Interim reanalysis data (Dee et al., 2011) as described in Ma et al. (2015).
143 Comprehensive observational data associated with mixed-phase cloud macrophysical and
144 microphysical properties are obtained from M-PACE and are used in the model evaluation.
145 Sensitivity experiments are performed to understand the individual impact of CNT, CLUBB, and
146 MG2 on EAMv1 simulated Arctic single-layer mixed-phase clouds. The remaining text is
147 organized as follows. Section 2 provides details about EAMv1, particularly its parameterizations
148 related to mixed-phase clouds, model experiments, and observation data. Section 3 discusses the
149 simulated mixed-phase clouds and their microphysical properties. Section 4 presents a detailed
150 process analysis. Conclusions and discussions are given in Section 5.

151

152 2. Model, model experiments, and observation data

153 2.1. EAMv1

154 EAMv1 was developed from CAM5 with notable changes to its physical
155 parameterizations. Its vertical resolution was also increased from 30 layers (used in CAM5) to 72
156 layers with 17 vertical layers are below 1.5 km. The updated physics package includes a
157 simplified third-order turbulence closure parameterization (CLUBB) (Golaz et al., 2002; Larson,
158 2017; Larson & Golaz, 2005) that unifies the treatment of planetary boundary layer turbulence,
159 shallow convection, and cloud macrophysics to remove the unrealistic separation of these
160 physical processes, which is characteristic of most climate models. CLUBB achieves the high-
161 order closure through a set of triple joint probability density function (PDF) of vertical velocity
162 | (w), liquid water potential temperature (θ_l), and total specific water content (q_t). A double
163 | Gaussian function is assumed to define the shape of trivariate PDF. CLUBB predicts the
164 | variances and correlations between θ_l , q_t , and w , as well as the third moment $\overline{w'^3}$ to determine
165 | the parameters of the assumed joint PDF. Once the joint PDF is known, other higher-order
166 moments can be closed by integrating over the assumed PDF to achieve the closure in CLUBB
167 prognostic equations. Cloud quantities such as cloud fraction and cloud liquid water mixing ratio
168 can be diagnosed directly via the integration of joint PDF over the saturated portion (Larson et
169 al., 2002). We note that the current CLUBB scheme is only designed for warm cloud processes.
170 Ice phase processes are not explicitly included in the CLUBB's PDF approach. Ice cloud fraction
171 is determined in EAMv1 based on the relative humidity (Gettelman et al., 2010). Cloud ice mass
172 mixing ratio, on the other hand, is transported via a turbulence eddy diffusion scheme
173 (Bogenschutz et al., 2013).

174 The MG2 two-moment cloud microphysical scheme (Gettelman & Morrison, 2014) is
175 also incorporated into EAMv1. The new scheme prognoses the mass and number mixing ratios
176 of snow and rain hydrometeors to replace the diagnostic treatment in MG1 (Morrison &
177 Gettelman, 2008). To better couple with the CLUBB parameterization, sub-time steps of 5 min
178 are used in the cloud microphysics. Furthermore, EAMv1 adopts the CNT to represent
179 immersion, contact, and deposition heterogeneous freezing in the mixed-phase cloud regime
180 (Wang et al., 2014). CNT links the ice particle formation to aerosol (i.e., dust and soot)
181 properties such as the aerosol number concentration and particle size (Hoose et al., 2010). Other
182 physical parameterizations used in EAMv1 include the four-mode version of modal aerosol
183 module (MAM4) (Liu et al., 2016) and Zhang and McFarlane (1995) deep convection scheme.

184

185 **2.2. Model experiments**

186 Table 1 lists the model experiments conducted in this study to understand the impact of
187 each individual change on EAMv1 simulated Arctic mixed-phase clouds. The control experiment
188 (“CTL”) has the same model configuration as default EAMv1, except that we remove the
189 artificial parameter that is applied to the WBF process. This is also the case for all the sensitivity
190 experiments. In this way, we can emphasize our study on the impact of changes in model
191 physical parameterizations on simulated Arctic mixed-phase clouds. In “MEYERS”, the Meyers
192 et al. (1992) heterogeneous ice nucleation parameterization replaces the CNT scheme in CTL. As
193 nucleated ice particle number concentrations largely differ between the two schemes, this
194 experiment is designed to understand how different heterogeneous nucleation schemes would
195 influence the partitioning of condensed cloud water in EAMv1. The experiment “UW” replaces

196 the CLUBB with the CAM5 University of Washington (UW) PBL turbulence scheme
197 (Bretherton & Park, 2009), shallow convection scheme (Park & Bretherton, 2009), and cloud
198 macrophysics scheme (Park et al., 2014), which is used to study the impact of CLUBB on the
199 simulated SLF. Finally, in the experiment “UW_MG1”, the MG2 two-moment cloud
200 microphysics is further changed to MG1 based on the experiment “UW”. By comparing the
201 “UW” with “UW_MG1”, the impact of prognostic treatment of precipitating hydrometeors on
202 simulated mixed-phase clouds can be analyzed. We note that we use EAMv1 as the baseline,
203 because we want to trace back which parameterization changes that have been made during the
204 EAMv1 development are responsible for the model behavior change. EAMv1 provides the
205 option for the user to switch back to certain old parameterizations without too much effort
206 involved.

207 For each experiment, a series of 3-day hindcasts (Ma et al., 2015) are initialized every
208 day from 30 September 2004 to 31 October 2004 to cover the M-PACE period. The initial
209 conditions of large-scale states (i.e., horizontal wind, temperature, and water vapor) are from the
210 ERA-Interim reanalysis. To avoid potential problems associated with model initial spin-up and
211 surface types, Day 2 (24 - 48 hr) hindcasts at the land grid point that is closest to the ARM NSA
212 Barrow observation site (71.3°N, 156.6°W) are extracted and used for our analysis.

213

214 **2.3. M-PACE observations**

215 Table 2 summarizes the observational data used for model evaluation in this study. The
216 cloud microphysical properties were retrieved using different algorithms as summarized in the
217 ARM cloud retrieval ensemble dataset (ACRED) (Zhao et al., 2012). ACRED provides a rough

218 estimate of uncertainties in derived cloud microphysical properties that are attributed to the
219 retrieval techniques. For M-PACE, five different retrieval products are available, which are
220 either from the ARM baseline retrievals (MICROBASE) or from individual research groups (See
221 Zhao et al., 2012 for more details). The hourly-averaged ACRED data in October 2004 is used
222 for validating the short-term hindcast results.

223 Other observational data comprises the frequency of cloud occurrence based on the
224 integrated measurements from ARM cloud radars, lidars, and laser ceilometers with the Active
225 Remotely Sensed Clouds Locations (ARSCL) algorithm (Clothiaux et al., 2000), and in-situ
226 measurements of the microphysical properties of single-layer boundary layer mixed-phase clouds
227 from the University of North Dakota (UND) Citation aircraft between 9 - 12 October 2004
228 (McFarquhar et al., 2007). During the M-PACE field campaign, four flights were conducted to
229 measure the cloud microphysical properties of single-layer boundary layer mixed-phase clouds.
230 Each flight lasted for 1 - 2 hours with cloud data collected every 10s.

231

232 **3. Results**

233 **3.1. Modeled mixed-phase clouds**

234 Figure 1 compares the time-pressure cross sections of the ARM observed cloud
235 frequency of occurrence at the NSA Barrow site and modeled grid-mean cloud fraction from the
236 day-2 hindcasts. Multi-layer mixed-phase clouds were observed between 5 - 8 October 2004,
237 whereas single-layer boundary layer mixed-phase clouds existed for the following 6-day period
238 (9 - 14 October). Maximum cloud fraction was observed at ~900 hPa. High clouds associated

239 with frontal systems dominated the last period of the M-PACE field campaign. The single-layer
240 low-level mixed-phase clouds from 9 to 14 October is a classic example of the Arctic mixed-
241 phase clouds that are ubiquitous over the Arctic region. In the following discussion, we will
242 emphasize our analysis on the single-layer mixed-phase clouds to understand how the changes in
243 physical parameterizations in EAMv1 affect their simulations.

244 Figure 1b shows that CTL simulates the resilient low-level single-layer mixed-phase
245 clouds between 9 - 14 October reasonably well. The cloud lifetime and temporal evolution, as
246 well as the cloud top height are also captured by the model. The simulated cloud base, however,
247 is slightly lower than the observations. We note that the cloud base (top) are defined as the
248 lowest (highest) level with non-zero cloud fraction simulated in the model. In general, the
249 simulated maximum cloud fraction shows little sensitivity to the parameterization changes
250 during the examined time period (Figures 1c, 1d, and 1e). In contrast, the simulated cloud
251 boundary is quite sensitive to the examined parameterizations. For example, the ice nucleation
252 scheme changed from the Meyers scheme to CNT leads to an increased cloud base height, closer
253 to the observations (Figure 1c), while using CLUBB to replace the UW schemes results in a
254 lower cloud base (Figure 1d). As cloud fraction is determined via the relative humidity in UW
255 cloud macrophysics scheme (Park et al., 2014), the clearer separation between cloud base and
256 surface below 950 hPa in UW is mostly attributed to the drier atmosphere near the surface (not
257 shown). For cloud microphysical parameterizations, the MG2 microphysics largely improves
258 cloud base height as indicated in Figure 1e compared to MG1.

259 Although the overall cloud structure is reasonably produced for the single-layer mixed-
260 phase clouds, large impacts from different model physical schemes are found on the simulated

261 liquid water and ice water mass mixing ratios. Figure 2 shows the modeled LWC, IWC, and SLF
262 in the CTL and the three sensitivity experiments. Note that the rain and snow water mass mixing
263 ratios are added to LWC and IWC, respectively, to better compare with the observations which
264 cannot distinguish them. One unexpected result shown in Figure 2 is that CTL simulates almost
265 no ice water mass mixing ratio in the mixed-phase clouds during 9 - 14 October. Supercooled
266 liquid water constitutes nearly all the condensed water mass mixing ratio for the persistent
267 single-layer low-level mixed-phase clouds at temperatures about -14°C (Figures 2a and 2e). SLF
268 is therefore close to 1 for these clouds (Figure 2i). This model behavior is in contrast to the
269 previous M-PACE studies with CAM5 where cloud ice water was commonly overestimated
270 while cloud liquid water was significantly underestimated (Liu et al., 2011; Xie et al., 2008,
271 2013). Since the artificial tuning parameter for the WBF process is removed in CTL, the
272 significant underestimation of IWC for the single-layer mixed-phase clouds is most likely a
273 result of too little ice being produced in the low-level mixed-phase clouds as we will discuss later.

274 Compared to CTL, more IWC is produced in MEYERS, indicating that the use of CNT in
275 EAMv1 leads to fewer IWC simulated for the single-layer mixed-phase clouds. Shi and Liu
276 (2019) found that this was due to the lower number concentration of ice particles formed from
277 the CNT heterogeneous ice nucleation while Meyers et al. overestimates INP number
278 concentrations compared to observations (DeMott et al., 2010). The use of CLUBB also plays an
279 important role on the decrease of cloud ice by comparing CTL and UW (Figures 2e and 2g).
280 MG2 microphysics slightly reduces IWC and increases LWC by comparing UW and UW_MG1
281 (Figures 2c and 2g with Figures 2d and 2h). This is because MG2 microphysics tends to have a
282 higher accretion rate of cloud liquid by rain than MG1. The conversion from cloud liquid to ice

283 then becomes weaker as more liquid is collected by rain drops. Moreover, compared to CTL,
284 UW_MG1 substantially decreases LWC and increases IWC in the modeled single-layer mixed-
285 phase clouds. The partitioning pattern between LWC and IWC in UW_MG1 is similar to what
286 was shown in CAM5 (Liu et al., 2011; Xie et al., 2013), although CNT is used in the UW_MG1
287 experiment. When Meyers et al. ice nucleation scheme is used in UW_MG1, more IWC and less
288 LWC are produced (not shown), making UW_MG1 more comparable to CAM5. Nevertheless,
289 the similarity between UW_MG1 (using either Meyers et al. or CNT scheme) and CAM5
290 demonstrates that the change of model dynamic core, vertical and horizontal resolutions, and
291 model tuning should not be the important reasons for the significant underestimated IWC in this
292 single-layer mixed-phase cloud case.

293 Figure 2 also shows the time-pressure cross sections of SLF for modeled mixed-phase
294 clouds. It is shown that the distribution of high SLF (close to 1) corresponds well with LWC.
295 Less spatial occurrence of high SLF is simulated in the single-layer mixed-phase clouds when
296 Meyers et al. ice nucleation, UW parameterizations, and MG1 cloud microphysics are used,
297 respectively.

298 Consistent with the lack of total cloud ice mass mixing ratio, a very low number
299 concentration ($< 0.01 \text{ L}^{-1}$) of cloud ice particles is produced in CTL between 9 - 14 October for
300 single-layer boundary layer mixed-phase clouds, particularly at temperatures between -10°C and
301 -15°C (Figure 3). It is clear that all the three changes of physical parameterizations tend to
302 decrease the ice particle number concentration as shown in Figures 3b-3d. Substantially more ice
303 crystals are produced after replacing the new schemes (i.e., CNT, CLUBB, and MG2) with old
304 ones (i.e., Meyers, UW, and MG1), and CLUBB and MG2 have stronger impacts than CNT.

305 Figure 4 compares modeled LWP and IWP to various retrievals contained in the ARM
306 ACRED data product. In general, differences are smaller in liquid phase retrievals among
307 different retrieval algorithms compared to those in ice phase retrievals. One to two orders of
308 magnitude differences can be found in the retrieved IWP, which could be the result of different
309 assumptions made in the IWP retrieval algorithms (Zhao et al., 2012). Compared to the ground-
310 based retrievals, CTL overpredicts LWP by a factor of 2 - 3 during more than half of the M-
311 PACE time, especially during 10 - 13 October when the low-level boundary layer mixed-phase
312 clouds were observed. Regarding IWP, it is shown that CTL underestimates the observed IWP
313 by 3 - 5 orders of magnitude during 9 - 14 October. When comparing sensitivity experiments to
314 CTL, we note that less LWP and more IWP are simulated given a particular suite of
315 parameterizations.

316 Figure 5 shows the comparison of SLF as a function of normalized cloud height between
317 in-situ measurements from the UND Citation aircraft and the EAM hindcast experiments. Note
318 that cloud altitude is normalized from 0 at cloud base to 1 at cloud top for both the observations
319 and model results, where modeled clouds are defined when total cloud water mass mixing ratios
320 are larger than 0.001 g kg^{-1} . The in-situ measurements were obtained on 9, 10, and 12 October
321 during the M-PACE field campaign to capture the vertical structures of single-layer mixed-phase
322 clouds and their microphysical properties (i.e., LWC and IWC). There were two flights on 9
323 October, and one flight on 10 and 12 October, respectively. In Figure 5, as we plot the in-situ
324 observations based on the date, so we combine the two flights on 9 October using the same color.
325 The aircraft data were processed by McFarquhar et al. (2007).

326 The aircraft measurements (Figure 5a) show that the observed SLF increases with
327 normalized cloud height and is larger than 80% near the cloud top. Larger fraction of cloud ice is
328 observed in the lower portion of clouds as lower SLF is found near the cloud base. The vertical
329 distribution of SLF is similar among the four research flights. Consistent with earlier discussion,
330 Figure 5b shows that CTL significantly overestimates SLF in the single-layer mixed-phase
331 clouds. The simulated SLF remains close to 100% for all cloud layers during the examined time
332 period. Compared to CTL, MEYERS better reproduces the vertical distribution of SLF in the
333 observations, but its SLF near the cloud base tends to be underestimated compared to
334 observations. This underestimation is probably because we include total water mass mixing ratio
335 to define the cloud base in our sampling strategy. As high ice particle number concentration is
336 generated from the Meyers et al. ice nucleation parameterization near the cloud base, cloud ice
337 water dominates the sampled cloud base in MEYERS. It is clearly shown in Figure 2b and 2f that
338 cloud liquid water tends to distribute separately from cloud ice water in modeled clouds. Figure
339 5d shows that the increasing SLF pattern with normalized cloud height is well captured by UW
340 on 10 and 12 October, while such trend is poorly simulated on 9 October. Too much cloud ice
341 water is simulated near the cloud base on 9 October. We note that 9 October is a transition period
342 in terms of the large-scale synoptic conditions during the M-PACE campaign. A high pressure
343 system was built over the pack ice to the northeast of Alaska coast and brought cooled air to the
344 Barrow site, largely decreasing surface temperature during 9 October (Verlinde et al., 2007). The
345 overestimated cloud ice mass shown in UW may be explained by the inadequate representation
346 of this transition in the UW schemes. In contrast to UW, UW_MG1, which replaced MG2 with
347 MG1, does not capture the increasing pattern of simulated SLF on 10 and 12 October, indicating

348 the use of MG2 microphysics is able to improve the SLF vertical distribution of modeled single-
349 layer mixed-phase clouds.

350

351 **4. Mass budget analysis**

352 To better understand which cloud microphysical processes play the most important role
353 in the changes of model behavior in simulating mixed-phase cloud phases in EAMv1 compared
354 to CAM5, in this section we further analyze the detailed cloud microphysical budgets for the four
355 hydrometeors -- cloud liquid, cloud ice, rain, and snow -- for the single-layer mixed-phase clouds
356 during the period between 9 - 11 October. The budget terms are the vertical integrals of
357 microphysical process tendencies over the selected time period.

358

359 **4.1. Impact of heterogeneous ice nucleation**

360 Figure 6a shows that liquid water condensation constitutes the majority of cloud liquid
361 water source in both CTL and MEYERS. Note that the amount of condensed liquid water is
362 directly diagnosed from the assumed joint PDF in the CLUBB parameterization (Bogenschutz et
363 al., 2012; Golaz et al., 2002). Although three orders of magnitude difference are found in the
364 number concentration of nucleated ice particles between CTL and MEYERS (figure not shown),
365 comparable liquid condensation tendencies are found in both experiments. This suggests that
366 different heterogeneous ice nucleation schemes have minimal impacts on the liquid water
367 formation.

368 It is interesting to notice that even though cloud ice and snow mass mixing ratios are
369 negligible in the single-layer mixed-phase clouds between 9 and 11 October in CTL, ice phase
370 associated microphysical processes remains active at limited rates. For instance, the WBF
371 process with respect to ice and snow and the snow accretion of liquid droplets are weakly
372 activated to transfer formed liquid water to ice and snow. However, almost all the generated
373 cloud ice water is converted to snow via autoconversion (Figure 6c). Snow water then tends to
374 sediment out of clouds, leaving negligible amount of total ice water mass mixing ratio in CTL
375 simulated mixed-phase clouds. Comparing MEYERS to CTL, with the higher ice particle
376 number concentration from the heterogeneous ice production, larger tendencies of ice associated
377 processes are shown in MEYERS. In particular, the WBF process rate with respect to ice is
378 largely increased, which leads to the larger cloud ice mass mixing ratio. As the growth of snow
379 water mass mixing ratio is strongly influenced by the autoconversion of cloud ice, larger snow
380 growth rates such as the WBF process with respect to snow and snow accretion of liquid droplets
381 are shown in Figure 6d in MEYERS. Meanwhile, the different ice number concentration also
382 changes the pathway of whether liquid droplets are collected by rain drops or snow particles. For
383 example, when higher ice number concentration is formed by MEYERS, more liquid droplets are
384 collected by snow, substantially inhibiting the accretion of liquid droplets by rain drops (Figure
385 6b). This further increases the ratio of ice water mass mixing ratio to liquid water mass mixing
386 ratio. Therefore, the number concentration of ice particles generated from heterogeneous ice
387 production is important for the Arctic single-layer mixed-phase clouds. The heterogeneous ice
388 production from the CNT scheme in CTL is too weak at temperatures warmer than -15°C . We
389 note that the impact of heterogeneous ice production on simulated mixed-phase clouds is

390 important more through its influence on cloud ice number concentration, not on ice mass mixing
391 ratio. As shown in Figure 6a, the mass tendency for heterogeneous ice nucleation is significantly
392 small. This is because the mass of newly formed ice crystals is so small that they cannot have a
393 comparable mass tendency to other processes such as the WBF process. However, this does not
394 impair the importance of heterogeneous ice nucleation as the ice particle number concentration
395 impacts cloud ice growth processes such as WBF.

396

397 **4.2. Impact of CLUBB**

398 Comparing UW to CTL, the change of cloud physical processes in the simulated mixed-
399 phase clouds due to the use of CLUBB can be analyzed. In the UW experiment, the liquid
400 condensation is determined by cloud macrophysics (Park et al., 2014), and the shallow
401 convection is calculated by Park and Bretherton (2009). When shallow convection is separately
402 treated in the UW parameterization, liquid mass mixing ratio detrained from shallow convection
403 is of comparable magnitude to the condensation (Figure 6a). However, it is no longer able to
404 diagnose the detrainment and condensation processes separately in CTL, since CLUBB
405 implicitly calculates the total production of cloud liquid water via the integral over saturated
406 portion of the joint PDF (Golaz et al., 2002; Larson et al., 2002).

407 Similar to the cloud liquid water mass budget, detrainment from shallow convection also
408 constitutes the source for cloud ice mass mixing ratio when CLUBB is not used (Figure 6c).
409 Such detrained cloud ice particles, together with the nucleated ice particles from heterogeneous
410 ice nucleation, participate in the cloud ice mass growth. We emphasize the importance of the

411 initial amount of cloud ice (either from shallow convection detrainment or from heterogeneous
412 ice nucleation) here, because one prerequisite for the ice mass growth is that it requires the
413 modeled clouds to contain sufficient cloud ice at the beginning. As noted in section 2.1, ice
414 phase related processes are currently not explicitly treated in CLUBB's PDF method. Instead, ice
415 mass mixing ratio is transported to CLUBB through an eddy diffusion scheme. Such an eddy
416 diffusion transport, however, is found to be inactive in the examined low-level boundary layer
417 mixed-phase clouds (shown in Figure 6c). Without the initial ice from shallow convection when
418 CLUBB is used, the further increase of cloud ice mass mixing ratio is substantially weaker in
419 CTL when compared to UW, such as the WBF process with respect to ice.

420 Meanwhile, it is shown in Figure 6c that the growth of ice crystals through water vapor
421 deposition also contributes to the cloud ice mass mixing ratio in UW, but this source is not
422 evident in CTL. In the MG stratiform cloud microphysical parameterization, ice depositional
423 growth is parameterized as two separate processes. The WBF process is one of them, which
424 represents the conversion of cloud liquid water to ice (and snow) assuming homogeneous mixing
425 between liquid and ice (and snow) in each grid cell at subfreezing temperatures. Since the MG
426 microphysics does not treat the evaporation of cloud liquid water, the real WBF process that
427 liquid droplets evaporate first and then water vapor deposits on ice crystals is not numerically
428 represented. When abundant cloud ice coexists with cloud liquid in mixed-phase clouds, the
429 WBF process will first be activated to consume available liquid water in the MG microphysics.
430 Under the circumstance that cloud liquid water is totally consumed within one model time step
431 (5 minutes, as sub-step is used in cloud microphysics), ice crystals will then continue their
432 growth at the expense of water vapor until the end of that sub-step. The latter process is invoked

433 as ice depositional growth in the MG microphysics. Therefore, the indication of ice deposition in
434 UW implies that all available liquid water in the simulated single-layer mixed-phase clouds is
435 completely consumed at certain levels or at certain time steps, but such a total consumption
436 never occurs in CTL because of the weak growth rate of ice particles. Furthermore, because of
437 the larger source for ice mass mixing ratio in UW, snow water also becomes more abundant via
438 autoconversion of cloud ice. Accretion of rain and ice by snow particles is enhanced, which
439 further increases the amount of ice phase cloud condensates in modeled mixed-phase clouds.

440 Therefore, in CTL modeled single-layer low-level mixed-phase clouds, the CLUBB
441 parameterization significantly underestimates one source of cloud ice water that is represented in
442 Park and Bretherton (2009). Such underestimation of cloud ice largely reduces the initial amount
443 of ice particles that grow through the following cloud microphysical processes. Increases of
444 cloud ice and snow mass mixing ratios are then substantially inhibited, resulting in an
445 underestimation of total ice mass mixing ratio.

446

447 **4.3. Impact of MG2**

448 The impact of cloud microphysical parameterization change from MG1 to MG2 can be
449 examined by comparing UW and UW_MG1 experiments. In general, the use of MG2 reduces the
450 process tendencies for ice and snow growth at the expense of cloud liquid water. For example,
451 the WBF process with respect to both ice and snow, as well as the snow accretion of liquid
452 droplets become substantially weaker in UW than UW_MG1. These changes can be mostly
453 attributed to the prognostic treatment of precipitation hydrometeors (rain and snow) in the MG2

454 microphysics. Another important aspect in MG2 modeled clouds lies in the higher accretion rate
455 of liquid droplets by rain drops as shown in Figure 6a and 6b. Although total cloud ice mass
456 mixing ratio is largely reduced in the simulated mixed-phase clouds with MG2 microphysics,
457 there is no significant change in the formation of initial cloud ice amount. For example, the
458 heterogeneous ice nucleation is the same between UW and UW_MG1. The detrained cloud ice
459 from shallow convection also behaves similarly. Therefore, the change of cloud microphysics
460 should not be as important as the other two parameterization changes. Nevertheless, as noted in
461 Gettelman et al. (2014), MG2 simulated mixed-phase clouds are strongly sensitive to the ice
462 particle number concentration. The change of initial ice source can then have a stronger impact
463 on the cloud microphysical processes in MG2 than MG1.

464

465 **5. Summary and discussions**

466 In this study, we utilize the short-term hindcast approach to understand which physical
467 process is most responsible for the significant behavior change in modeled high-latitude single-
468 layer mixed-phase clouds in the U.S. DOE E3SM atmospheric model (EAMv1) compared to its
469 predecessor, CAM5. The hindcast approach allows us to isolate model deficiencies in its
470 physical parameterizations and to compare model results directly to field campaign observations.
471 A series of short-term hindcasts with EAMv1 are conducted for the DOE ARM Mixed-Phase
472 Arctic Cloud Experiment (M-PACE) field campaign period when well-defined single-layer
473 mixed-phase clouds were observed during 9 - 14 October 2004 at the ARM NSA site. Day-2
474 hindcast results are utilized to compare with observational data collected during M-PACE. We

475 find that the simulated single-layer boundary layer mixed-phase clouds are overly dominated by
476 supercooled liquid water in the default EAMv1. Such a model behavior is dramatically different
477 from CAM5. Compared to CAM5, EAMv1 has adopted a few major changes in the physical
478 parameterizations, and these parameterizations can largely alter the model performance on the
479 mixed-phase cloud phase partitioning. In this study, three parameterizations are targeted,
480 including the use of CNT heterogeneous ice nucleation scheme; the CLUBB scheme which
481 unifies shallow convection, PBL turbulence, and cloud macrophysics in a unified framework; as
482 well as the MG2 cloud microphysics which prognostically treats the number and mass mixing
483 ratios of precipitation hydrometeors. Three sensitivity experiments are performed to isolate the
484 individual effect of the aforementioned schemes on simulated single-layer mixed-phase cloud
485 properties.

486 The hindcast results show that too little total ice water mass mixing ratio is produced in
487 the default EAMv1 for the single-layer boundary layer mixed-phase clouds during the M-PACE.
488 On the other hand, total liquid water mass mixing ratio is overestimated when compared with the
489 ARM ground-based remote sensing data. By tracing back the changes made in EAMv1, we find
490 that the CNT ice nucleation scheme, CLUBB parameterization, and MG2 cloud microphysics all
491 tend to decrease cloud ice mass mixing ratio, respectively. When all three schemes are combined
492 together, the decreased cloud ice resulted from individual scheme change tends to add up,
493 leading to a significant decrease of cloud ice amount and a significant increase of cloud liquid
494 amount in modeled single-layer Arctic mixed-phase clouds. The detailed budget analysis of
495 cloud microphysical process tendencies indicates that the initial ice particles are critical for the
496 increase of total ice mass in the following cloud microphysics. Two important processes, the

497 heterogenous ice nucleation and the detrainment of cloud ice from shallow convection, produce a
498 minimal number of initial ice particles when EAMv1 uses CNT and CLUBB to respectively
499 replace the Meyers et al. ice nucleation scheme and the UW shallow convection and turbulence
500 parameterizations used in CAM5. As the mass growth rate of ice crystals depends sensitively on
501 the number concentration of ice particles in cloud microphysics, cloud ice mass is largely
502 reduced. For example, the WBF process with respect to ice is much weaker in CTL compared
503 with the three sensitivity experiments. In addition, the formation of snow water is also reduced in
504 CTL, which leads to a weaker collection of liquid droplets, rain drops, and ice particles by snow.
505 As the use of MG2 does not impact the initial ice crystals, the MG2 cloud microphysics should
506 not be a primer reason for the underestimation of cloud ice. However, the introduction of MG2
507 significantly reduces the WBF process with respect to both ice and snow, and the snow accretion
508 of liquid, which also results in a lower total ice mass.

509 We note that the issue analyzed in this paper is more related to the Arctic single-layer
510 boundary layer mixed-phase clouds. In particular, the insufficient ice formation from the CNT
511 heterogeneous ice production is more problematic for mixed-phase clouds at temperatures
512 warmer than -15°C . With the CNT ice nucleation linked to aerosol properties, the model
513 deficiency in aerosol fields can be passed to the modeled mixed-phase clouds. EAMv1, like
514 many other GCMs, underestimates the dust transport from mid-latitude sources and Arctic local
515 dust sources, and neglects biological aerosols. This leads to the substantial underestimation of
516 INP number concentrations over the Arctic (Shi & Liu, 2019). Such biases in modeled aerosols
517 and INPs contribute to the biased phase partitioning of high latitude mixed-phase clouds in
518 EAMv1. To address the issue in the CLUBB parameterization, including the phase partitioning

519 of CLUBB condensed cloud water in a similar approach as Park and Bretherton (2009) may help
520 to increase the initial ice that passes to the MG2 microphysics. Ice phase should also be
521 considered in the CLUBB's PDF parameterization in order to develop a unified framework for
522 shallow convection, PBL turbulence, and cloud macrophysics for cold clouds. Moreover, other
523 cloud microphysical processes important for the increase of cloud ice mass may not be
524 parameterized in the MG2 cloud microphysics. For example, the secondary ice production is too
525 weak in the current modeled mixed-phase clouds.

526 Although this study is based on an analysis of the M-PACE field campaign at one single
527 location, the overly dominated cloud liquid water tends to be a common phenomenon beyond
528 this ARM site in EAMv1 modeled mixed-phase clouds (figures not shown). Results from a
529 global evaluation of EAMv1 simulated mixed-phase clouds will be reported in a separate paper.
530 As indicated in earlier studies, mixed-phase cloud feedback and climate sensitivity can be
531 strongly influenced by the mixed-phase cloud phase partitioning (Tan & Storelvmo, 2019; Tan et
532 al., 2016). How the biased phase partitioning of condensed cloud water in low-level mixed-phase
533 clouds identified in this study would impact the cloud feedback and climate sensitivity estimated
534 by E3SM is of interest to understand in the future study. Due to the ubiquitous distribution of this
535 type of clouds in mid- and high latitudes, how to improve the mixed-phase cloud phase
536 partitioning simulated in GCMs is still an open question for the community. Attempts can be
537 either from the aerosol aspect or cloud microphysics aspect to address the outstanding problems.

538

539 **Acknowledgement:** This research was primarily supported by the DOE Atmospheric System
540 Research (ASR) Program (grants DE-SC0014239 and DE-SC0018926) and the Energy Exascale
541 Earth System Model (E3SM) project and partially funded by the DOE Regional and Global
542 Model Analysis program area (RGMA) and ASR's Cloud-Associated Parameterizations Testbed
543 (CAPT) project and the Climate Model Development and Validation (CMDV) activity, funded
544 by the U.S. Department of Energy, Office of Science, Office of Biological and Environmental
545 Research. The model data used in this study can be downloaded at
546 <http://portal.nersc.gov/project/m2136/E3SMv1/Zhang-SLF>. Work at LLNL was performed under
547 the auspices of the U.S. DOE by Lawrence Livermore National Laboratory under contract No.
548 DE-AC52-07NA27344. The Pacific Northwest National Laboratory (PNNL) is operated for the
549 DOE by Battelle Memorial Institute under contract DE-AC06-76RLO 1830. This research used
550 high-performance computing resources from the National Energy Research Scientific Computing
551 Center, a DOE Office of Science User Facility supported by the Office of Science of the U.S.
552 Department of Energy under Contract No. DE-AC02-05CH11231. The ARM M-PACE
553 observational dataset is available from DOE ARM website
554 (<https://www.archive.arm.gov/discovery/>).

555

556 **Table and Figures**557 Table 1. *Summary of Physical Parameterizations in EAMv1 Simulations*

Experiment	Configurations	Note
CTL	Parameter “berg_eff_factor” change to 1.0	Same as default EAMv1, but use the value 1.0 for the parameter that controls the WBF rate.
MEYERS	Same as CTL, but replace the CNT ice nucleation scheme (Wang et al., 2014) with Meyers et al. (1992)	Examine the effect of heterogeneous ice nucleation. Note that the Meyers scheme generally produces higher INP number concentrations than CNT.
UW	Same as CTL, but replace CLUBB with the CAM5 UW shallow convection, PBL turbulence, and cloud macrophysical schemes (Park and Bretherton, 2009; Bretherton and Park 2009; Park et al. 2014)	Examine the effect of CLUBB.
UW_MG1	Same as UW, except using the MG1 microphysics	Examine the effect of updated cloud microphysics.

558

559 Table 2. *Summary of M-PACE Observations Used in This Study*

Observation	Quantity	Source and reference
ACRED	LWC/LWP and IWC/IWP	ARM cloud retrieval ensemble dataset (ACRED; Zhao et al., 2012)
ARSCL	Cloud fraction	Active Remotely Sensed Clouds Locations (ARSCL) algorithm (Clothiaux et al., 2000)
UND Citation	LWC and IWC	University of North Dakota (UND) Citation aircraft (McFarquhar et al., 2007)

560

561 Figure 1. Time-pressure cross sections of cloud fraction at the NSA Barrow site during the M-
562 PACE field campaign. (a) Observed frequency of occurrence of clouds from the Active
563 Remotely Sensed Clouds Locations (ARSCL) algorithm. (b) Simulated cloud fraction from CTL.
564 (c)-(e) are the differences in simulated cloud fraction between (c) CTL and MEYERS, (d) CTL
565 and UW, and (e) UW and UW_MG1. Unit: %. Note that CTL utilizes CLUBB, MG2, and CNT
566 parameterizations, while three sensitivity experiments have changes of Meyers et al. (1992) ice
567 nucleation (MEYERS), UW shallow convection, PBL turbulence, and cloud macrophysics
568 parameterizations (UW), and both UW schemes and MG1 cloud microphysics (UW_MG1),
569 respectively.

570

571 Figure 2. Time-pressure cross sections of simulated total cloud liquid water mass mixing ratio
572 (including rain water mass; upper panel), total cloud ice water mass mixing ratio (including snow
573 water mass; middle panel), and supercooled liquid fraction (lower panel) during the M-PACE
574 field campaign from CTL, MEYERS, UW, and UW_MG1 (from left to right). (a)-(d) are for

575 cloud liquid water, (e)-(h) are for cloud ice water mass, and (i)-(l) are for supercooled liquid
576 fraction. Contours represent the ambient temperature in the unit of °C.

577

578 Figure 3. Time-pressure cross sections of simulated grid mean cloud ice number concentrations
579 for the M-PACE. (a) CTL, (b) MEYERS, (c) UW, and (d) UW_MG1. Contours represent the
580 ambient temperature in the unit of °C.

581

582 Figure 4. Time series of liquid water path (including rain; upper panel) and ice water path
583 (including snow; lower panel) from the EAMv1 and the ARM ACRED dataset. CTL is presented
584 by red solid line, MEYERS green solid line, UW blue solid line, and UW_MG1 brown solid line.
585 For the ACRED dataset, red star is the MICROBASE observation. Green plus is the retrieval
586 from Shupe (2007). Purple cross represents the retrieval products from Wang et al., (2004). Dark
587 blue circle is from Dong and Mace (2003), and orange triangle is from Deng and Mace (2006).
588 Grey lines represent the one standard deviation for each data point.

589

590 Figure 5. Distribution of supercooled liquid fraction as a function of normalized height in clouds.
591 (a) The in-situ measurements obtained from the University of North Dakota Citation aircraft
592 (McFarquhar et al., 2007) on 9 October (black dots), 10 October (red dots), and 12 October (blue
593 dots) during the M-PACE field campaign. (b)-(e) Results of model simulations from CTL,
594 MEYERS, UW, and UW_MG1, respectively. Model results are sampled on 9, 10, 12 October
595 which correspond to the same time period as the measurements.

596

597 Figure 6. Budgets of vertically integrated cloud physical process tendencies of (a) cloud liquid,
598 (b) rain, (c) cloud ice, and (d) snow hydrometeors from the short-term hindcast day-2 results of
599 CTL (red bars) and three sensitivity experiments, which are MEYERS (green bars), UW (blue
600 bars), and UW_MG1 (brown bars). The vertically integrated process rates are averaged over 3-
601 day period between 9 and 11 October 2004 during the M-PACE field campaign.

602

603

604 **References**

605 Barrett, A. I., Hogan, R. J., & Forbes R. M. (2017). Why are mixed-phase altocumulus clouds
606 poorly predicted by large-scale models? Part 1. Physical processes. *Journal of Geophysical*
607 *Research: Atmospheres*, 122, 9903-9926. <https://doi.org/10.1002/2016JD026321>

608

609 Bennartz, R., Shupe, M. D., Turner, D. D., Walden, V. P., Steffen, K., Cox, C. J., et al. (2013).
610 July 2012 Greenland melt extent enhanced by low-level liquid clouds. *Nature*, 496, 83-86.
611 <https://doi.org/10.1038/nature12002>

612

613 Bogenschutz, P. A., Gettelman, A., Morrison, H., Larson, V. E., Craig, C., & Schanen, D. P.
614 (2013). Higher-order turbulence closure and its impact on climate simulations in the Community
615 Atmosphere Model. *Journal of Climate*, 26(23), 9655–9676. [https://doi.org/10.1175/JCLI-D-13-](https://doi.org/10.1175/JCLI-D-13-00075.1)
616 [00075.1](https://doi.org/10.1175/JCLI-D-13-00075.1)

617

618 Bogenschutz, P. A., Gettelman, A., Morrison, H., Larson, V. E., Schanen, D. P., Meyer, N. R., et
619 al. (2012). Unified parameterization of the planetary boundary layer and shallow convection with
620 a higher-order turbulence closure in the Community Atmosphere Model: single-column
621 experiments. *Geoscientific Model Development*, 5, 1407-1423. [https://doi.org/10.5194/gmd-5-](https://doi.org/10.5194/gmd-5-1407-2012)
622 [1407-2012](https://doi.org/10.5194/gmd-5-1407-2012), 2012

623

624 Bretherton, C. S. & Park, S. (2009). A New Moist Turbulence Parameterization in the
625 Community Atmosphere Model. *Journal of Climate*, 22, 3422-3448.
626 <https://doi.org/10.1175/2008JCLI2556.1>

627

628 Clothiaux, E. E., Ackerman, T. P., Mace, G. G., Moran, K. P., Marchand, R. T., Miller, M. A., &
629 Martner, B. E. (2000). Objective determination of cloud heights and radar reflectivities using a
630 combination of active remote sensors at the ARM CART sites. *Journal of Applied Meteorology*
631 *and Climatology*, 39, 645-665. [https://doi.org/10.1175/1520-](https://doi.org/10.1175/1520-0450(2000)039%3C0645:ODOCHA%3E2.0.CO;2)
632 [0450\(2000\)039%3C0645:ODOCHA%3E2.0.CO;2](https://doi.org/10.1175/1520-0450(2000)039%3C0645:ODOCHA%3E2.0.CO;2)

633

634 de Boer, G., Eloranta, E. W., & Shupe, M. D. (2009). Arctic Mixed-Phase Stratiform Cloud
635 Properties from Multiple Years of Surface-Based Measurements at Two High-Latitude
636 Locations. *Journal of the Atmospheric Science*, 66, 2874-2887.
637 <https://doi.org/10.1175/2009JAS3029.1>

638

639 Dee, D. P., Uppala, S. M., Simmons, A. J., Berrisford, P., Poli, P., Kobayashi, S., et al. (2011).
640 The ERA-Interim reanalysis: configuration and performance of the data assimilation system.
641 *Quarterly Journal of the Royal Meteorological Society*, 137, 553-597.
642 <https://doi.org/10.1002/qj.828>

643

644 DeMott, P. J., Prenni, A. J., Liu, X., Kreidenweis, S. M., Petters, M. D., Twohy, C. H., et al.
645 (2010). Predicting global atmospheric ice nuclei distributions and their impacts on climate.
646 *Proceedings of the National Academy of Sciences*, 107(25), 11217-11222. [https://doi.org/](https://doi.org/10.1073/pnas.0910818107)
647 10.1073/pnas.0910818107

648

649 DeMott, P. J., Prenni, A. J., McMeeking, G. R., Sullivan, R. C., Petters, M. D., Tobo, Y., et al.
650 (2015). Integrating laboratory and field data to quantify the immersion freezing ice nucleation
651 activity of mineral dust particles. *Atmospheric Chemistry and Physics*, 15(1), 393-409.
652 <https://doi.org/10.5194/acp-15-393-2015>

653

654 Deng, M., & Mace, G. (2006). Cirrus microphysical properties and air motion statistics using
655 cloud radar Doppler moments. Part I: Algorithm description. *Journal of Applied Meteorology*
656 *and Climatology*, 45, 1690-1709. <https://doi.org/10.1175/JAM2433.1>

657

658 Dong, X., & Mace, G. G. (2003). Profiles of low-level stratus cloud microphysics deduced from
659 ground-based measurements. *Journal of Atmospheric and Oceanic Technology*, 20, 42-53.
660 [https://doi.org/10.1175/1520-0426\(2003\)020<0042:POLLSC>2.0.CO;2](https://doi.org/10.1175/1520-0426(2003)020<0042:POLLSC>2.0.CO;2)

661

662 Gettelman, A., Liu, X., Ghan, S. J., Morrison, H., Park, S., Conley, A. J., et al. (2010). Global
663 simulations of ice nucleation and ice supersaturation with an improved cloud scheme in the
664 Community Atmosphere Model. *Journal of Geophysical Research: Atmospheres*, 115, D18216.
665 <https://doi.org/10.1029/2009JD013797>

666

667 Gettelman, A., & Morrison, H. (2014). Advanced two-moment bulk microphysics for global
668 models. Part I: Off-line tests and comparison with other schemes. *Journal of Climate*, 28(3),
669 1268-1287. <https://doi.org/10.1175/JCLI-D-14-00102.1>

670

671 Gettelman, A., Morrison, H., Santos, S., Bogenschutz, P. & Caldwell, P. M. (2015). Advanced
672 Two-Moment Bulk Microphysics for Global Models. Part II: Global Model Solutions and
673 Aerosol–Cloud Interactions. *Journal of Climate*, 28, 1288-1307. [https://doi.org/10.1175/JCLI-D-](https://doi.org/10.1175/JCLI-D-14-00103.1)
674 [14-00103.1](https://doi.org/10.1175/JCLI-D-14-00103.1)

675

676 Golaz, J.-C., Caldwell, P. M., Van Roekel, L. P., Petersen, M. R., Tang, Q., Wolfe, J. D., et al.
677 (2019). The DOE E3SM coupled model version 1: Overview and evaluation at standard
678 resolution. *Journal of Advances in Modeling Earth*
679 *Systems*, 11. <https://doi.org/10.1029/2018MS001603>

680

681 Golaz, J.-C., Larson, V. E., & Cotton, W. R. (2002). A PDF-based model for boundary layer
682 clouds. Part I: Method and model description. *Journal of the Atmospheric Sciences*, 59(24),
683 3540–3551. [https://doi.org/10.1175/1520-0469\(2002\)059<3540:APBMFB>2.0.CO;2](https://doi.org/10.1175/1520-0469(2002)059<3540:APBMFB>2.0.CO;2)

684

685 Hofer, S., Tedstone, A. J., Fettweis, X. & Bamber, J. L. (2019). Cloud microphysics and
686 circulation anomalies control differences in future Greenland melt. *Nature Climate Change*, 9,
687 523-528. <https://doi.org/10.1038/s41558-019-0507-8>

688

689 Hoose, C., Kristjánsson, J. E., Chen, J. P., & Hazra, A. (2010). A classical-theory-based
690 parameterization of heterogeneous ice nucleation by mineral dust, soot, and biological particles
691 in a global climate model. *Journal of the Atmospheric Sciences*, 67, 2483-2503.
692 <https://doi.org/10.1175/2010JAS3425.1>

693

694 Kay, J. E., Bourdages, L., Miller, N. B., Morrison, A., Yettella, V., Chepfer, H. &
695 Eaton, B. (2016). Evaluating and improving cloud phase in the Community Atmosphere Model
696 version 5 using spaceborne lidar observations, *Journal of Geophysical Research: Atmospheres*,
697 121, 4162-4176. <https://doi.org/10.1002/2015JD024699>

698

699 Klein, S. A., McCoy, R. B., Morrison, H., Ackerman, A. S., Avramov, A., Boer, G. d., et al.
700 (2009). Intercomparison of model simulations of mixed-phase clouds observed during the ARM

701 Mixed-Phase Arctic Cloud Experiment. I: single-layer cloud. *Quarterly Journal of the Royal*
702 *Meteorological Society*, 135: 979-1002. <https://doi.org/10.1002/qj.416>

703

704 Komurcu, M., Storelvmo, T., Tan, I., Lohmann, U., Yun, Y., Penner, J. E., et al. (2014). Inter-
705 comparison of the cloud water phase among global climate models, *Journal of Geophysical*
706 *Research: Atmospheres*, 119, 3372-3400. <https://doi.org/10.1002/2013JD021119>

707

708 Larson, V. E. (2017). CLUBB-SILHS: A parameterization of subgrid variability in the
709 atmosphere. *ArXiv:1711.03675 [Physics]*. Retrieved from <http://arxiv.org/abs/1711.03675>

710

711 Larson, V. E., & Golaz, J.-C. (2005). Using probability density functions to derive consistent
712 closure relationships among higher-order moments. *Monthly Weather Review*, 133(4), 1023-1042.
713 <https://doi.org/10.1175/MWR2902.1>

714

715 Larson, V. E., Golaz, J. & Cotton, W. R. (2002). Small-Scale and Mesoscale Variability in
716 Cloudy Boundary Layers: Joint Probability Density Functions. *Journal of the Atmospheric*
717 *Sciences*, 59, 3519-3539. [https://doi.org/10.1175/1520-](https://doi.org/10.1175/1520-0469(2002)059<3519:SSAMVI>2.0.CO;2)
718 [0469\(2002\)059<3519:SSAMVI>2.0.CO;2](https://doi.org/10.1175/1520-0469(2002)059<3519:SSAMVI>2.0.CO;2)

719

720 Lawson, P. R., & Gettelman, A. (2014). Impact of Antarctic clouds on climate. *Proceedings of*
721 *the National Academy of Sciences*, 111(51), 18156-18161.

722 <https://doi.org/10.1073/pnas.1418197111>

723

724 Liu, X., Ma, P.-L., Wang, H., Tilmes, S., Singh, B., Easter, R. C., et al. (2016). Description and
725 evaluation of a new four-mode version of the Modal Aerosol Module (MAM4) within version
726 5.3 of the Community Atmosphere Model. *Geoscientific Model Development*, 9(2), 505-522.

727 <https://doi.org/10.5194/gmd-9-505-2016>

728

729 Liu, X., Xie, S., Boyle, J., Klein, S. A., Shi, X., Wang, Z., et al. (2011). Testing cloud
730 microphysics parameterizations in NCAR CAM5 with ISDAC and M-PACE
731 observations. *Journal of Geophysical Research: Atmospheres*, 116, D00T11.

732 <https://doi.org/10.1029/2011JD015889>

733

734 Lohmann, U. & Neubauer, D. (2018). The importance of mixed-phase and ice clouds for climate
735 sensitivity in the global aerosol–climate model ECHAM6-HAM2. *Atmospheric Chemistry and*
736 *Physics*, 18, 8807-8828. <https://doi.org/10.5194/acp-18-8807-2018>

737

738 Ma, H.-Y., Chuang, C. C., Klein, S. A., Lo, M.-H., Zhang, Y., Xie, S., et al. (2015). An
739 improved hindcast approach for evaluation and diagnosis of physical processes in global climate
740 models. *Journal of Advances in Modeling Earth Systems*, 7, 1810-1827. [https://doi.org/10.1002/](https://doi.org/10.1002/2015MS000490)
741 2015MS000490

742

743 Ma, H.-Y., Xie, S., Klein, S. A., Williams, K. D., Boyle, J. S., Bony, S., et al. (2014). On the
744 correspondence between mean forecast errors and climate errors in CMIP5 models. *Journal of*
745 *Climate*, 27(4), 1781-1798. <https://doi.org/10.1175/JCLI-D-13-00474.1>

746

747 McCoy, D. T., Hartmann, D. L., Zelinka, M. D., Ceppi, P., & Grosvenor, D. P. (2015). Mixed-
748 phase cloud physics and Southern Ocean cloud feedback in climate models. *Journal of*
749 *Geophysical Research: Atmospheres*, 120, 9539-9554. <https://doi.org/10.1002/2015JD023603>

750

751 McCoy, D. T., Tan, I., Hartmann, D. L., Zelinka, M. D., & Storelvmo, T. (2016). On the
752 relationships among cloud cover, mixed-phase partitioning, and planetary albedo in
753 GCMs. *Journal of Advances in Modeling Earth Systems*, 8, 650-668.

754 <https://doi.org/10.1002/2015MS000589>

755

756 McFarquhar, G. M., Zhang, G., Poellot, M. R., Kok, G. L., McCoy, R., Tooman, T., et al. (2007).
757 Ice properties of single-layer stratocumulus during the Mixed-Phase Arctic Cloud Experiment: 1.

758 Observations. *Journal of Geophysical Research: Atmospheres*, 112, D24201.

759 <https://doi.org/10.1029/2007JD008633>

760

761 Meyers, M. P., DeMott, P. J., & Cotton, W. R. (1992). New primary ice-nucleation

762 parameterizations in an explicit cloud model. *Journal of Applied Meteorology and*

763 *Climatology*, 31, 708-721. <https://doi.org/10.1175/1520->

764 0450(1992)031<0708:NPINPI>2.0.CO;2

765

766 Morrison, H., & Gettelman, A. (2008). A new two-moment bulk stratiform cloud microphysics

767 scheme in the Community Atmosphere Model, version 3 (CAM3). Part I: Description and

768 numerical tests. *Journal of Climate*, 21(15), 3642-3659. <https://doi.org/10.1175/2008JCLI2105.1>

769

770 Morrison, H., McCoy, R. B., Klein, S. A., Xie, S., Luo, Y., Avramov, A., et al. (2009).

771 Intercomparison of model simulations of mixed-phase clouds observed during the ARM Mixed-

772 Phase Arctic Cloud Experiment. II: Multilayer cloud. *Quarterly Journal of the Royal*

773 *Meteorological Society*, 135: 1003-1019. <https://doi.org/10.1002/qj.415>

774

775 Nicolas, J. P., Vogelmann, A. M., Scott, R. C., Wilson, A. B., Cadeddu, M. P., Bromwich, D. H.,

776 et al. (2017). January 2016 extensive summer melt in West Antarctica favoured by strong El

777 Niño. *Nature Communications*, 8, 15799. <https://doi.org/10.1038/ncomms15799>

778

779 Niemand, M., Möhler, O., Vogel, B., Vogel, H., Hoose, C., Connolly, P., et al. (2012). A
780 Particle-Surface-Area-Based Parameterization of Immersion Freezing on Desert Dust
781 Particles. *Journal of the Atmospheric Sciences*, 69, 3077-3092. [https://doi.org/10.1175/JAS-D-](https://doi.org/10.1175/JAS-D-11-0249.1)
782 11-0249.1

783

784 Park, S., & Bretherton, C. S. (2009). The University of Washington shallow convection and
785 moist turbulence schemes and their impact on climate simulations with the Community
786 Atmosphere Model. *Journal of Climate*, 22, 3449-3469. <https://doi.org/10.1175/2008JCLI2557.1>

787

788 Park, S., Bretherton, C. S., & Rasch, P. J. (2014). Integrating Cloud Processes in the Community
789 Atmosphere Model, Version 5. *Journal of Climate*, 27, 6821-6856. [https://doi.org/10.1175/JCLI-](https://doi.org/10.1175/JCLI-D-14-00087.1)
790 D-14-00087.1

791

792 Phillips, T. J., Potter, G. L., Williamson, D. L., Cederwall, R. T., Boyle, J. S., Fiorino, M., et al.
793 (2004). Evaluating Parameterizations in General Circulation Models: Climate Simulation Meets
794 Weather Prediction. *Bulletin of the American Meteorological Society*, 85, 1903-
795 1916. <https://doi.org/10.1175/BAMS-85-12-1903>

796

797 Rasch, P. J., Xie, S., Ma, P.-L., Lin, W., Wang, H., Tang, Q., et al. (2019). An Overview of the
798 Atmospheric Component of the Energy Exascale Earth System Model. *Journal of Advances in*
799 *Modeling Earth Systems*, 11. <https://doi.org/10.1029/2019MS001629>

800

801 Shi, Y., & Liu, X. (2019). Dust radiative effects on climate by glaciating mixed-phase clouds.
802 *Geophysical Research Letters*, 46. <https://doi.org/10.1029/2019GL082504>

803

804 Shupe, M. D. (2007). A ground-based multi sensor cloud phase classifier. *Geophysical Research*
805 *Letters*, 34, L22809. <https://doi.org/10.1029/2007GL031008>

806

807 Shupe, M. D., Matrosov, S. Y., & Uttal, T. (2006). Arctic Mixed-Phase Cloud Properties
808 Derived from Surface-Based Sensors at SHEBA. *Journal of the Atmospheric Sciences*, 63, 697-
809 711. <https://doi.org/10.1175/JAS3659.1>

810

811 Shupe, M. D., Walden, V. P., Eloranta, E., Uttal, T., Campbell, J. R., Starkweather, S. M. et
812 al. (2011). Clouds at Arctic Atmospheric Observatories. Part I: Occurrence and Macrophysical
813 Properties. *Journal of Applied Meteorology and Climatology*, 50, 626-
814 644. <https://doi.org/10.1175/2010JAMC2467.1>

815

816 Storelvmo, T., Kristjánsson, J. E., Lohmann, U., Iversen, T., Kirkevåg, A., & Seland, Ø. (2008).
817 Modeling of the Wegener-Bergeron-Findeisen process—implications for aerosol indirect
818 effects. *Environmental Research Letters*, 3, 045001. [https://doi.org/10.1088/1748-](https://doi.org/10.1088/1748-9326/3/4/045001)
819 9326/3/4/045001

820

821 Tan, I., & Storelvmo, T. (2016). Sensitivity study on the influence of cloud microphysical
822 parameters on mixed-phase cloud thermodynamic phase partitioning in CAM5. *Journal of the*
823 *Atmospheric Sciences*, 73, 709-728. <https://doi.org/10.1175/JAS-D-15-0152.1>

824

825 Tan, I., & Storelvmo, T. (2019). Evidence of strong contributions from mixed-phase clouds to
826 Arctic climate change. *Geophysical Research Letters*, 46, 2894-2902.
827 <https://doi.org/10.1029/2018GL081871>

828

829 Tan, I., Storelvmo, T., & Zelinka, M. D. (2016). Observational constraints on mixed-phase
830 clouds imply higher climate sensitivity. *Science*, 352, 224-227.
831 <https://doi.org/10.1126/science.aad5300>

832

833 Verlinde, J., Harrington, J. Y., McFarquhar, G. M., Yannuzzi, V. T., Avramov, A., Greenberg, S.,
834 et al. (2007). The Mixed-Phase Arctic Cloud Experiment. *Bulletin of the American*
835 *Meteorological Society*, 88, 205-222. <https://doi.org/10.1175/BAMS-88-2-205>

836

837 Wang, Y., Liu, X., Hoose, C., & Wang, B. (2014). Different contact angle distributions for
838 heterogeneous ice nucleation in the Community Atmospheric Model version 5. *Atmospheric
839 Chemistry and Physics*, 14, 10411-10430. <https://doi.org/10.5194/acp-14-10411-2014>

840

841 Wang, Y., Zhang, D., Liu, X., & Wang, Z. (2018). Distinct contributions of ice nucleation, large-
842 scale environment, and shallow cumulus detrainment to cloud phase partitioning with NCAR
843 CAM5. *Journal of Geophysical Research: Atmospheres*, 123, 1132-1154.
844 <https://doi.org/10.1002/2017JD027213>

845

846 Wang, Z., Sassen, K., Whiteman, D. N., & Demoz, B. B. (2004). Studying altocumulus with ice
847 virga using ground-based active and passive remote sensors, *Journal of Applied Meteorology
848 and Climatology*, 43, 449-460. [https://doi.org/10.1175/1520-
849 0450\(2004\)043<0449:SAWIVU>2.0.CO;2](https://doi.org/10.1175/1520-0450(2004)043<0449:SAWIVU>2.0.CO;2)

850

851 Xie, S., Boyle, J., Klein, S. A., Liu, X., & Ghan, S. (2008). Simulations of Arctic mixed-phase
852 clouds in forecasts with CAM3 and AM2 for M-PACE. *Journal of Geophysical Research:*
853 *Atmospheres*, 113, D04211. <https://doi.org/10.1029/2007JD009225>

854

855 Xie, S., Lin, W., Rasch, P. J., Ma, P.-L., Neale, R., Larson, V. E., et al. (2018). Understanding
856 cloud and convective characteristics in version 1 of the E3SM atmosphere model. *Journal of*
857 *Advances in Modeling Earth Systems*, 10, 2618-2644. <https://doi.org/10.1029/2018MS001350>

858

859 Xie, S., Liu, X., Zhao, C., & Zhang, Y. (2013). Sensitivity of CAM5-Simulated Arctic Clouds
860 and Radiation to Ice Nucleation Parameterization. *Journal of Climate*, 26, 5981-5999.
861 <https://doi.org/10.1175/JCLI-D-12-00517.1>

862

863 Xie, S., Ma, H.-Y., Boyle, J. S., Klein, S. A., & Zhang, Y. (2012). On the correspondence
864 between short- and long-time-scale systematic errors in CAM4/CAM5 for the year of tropical
865 convection. *Journal of Climate*, 25(22), 7937-7955. <https://doi.org/10.1175/JCLI-D-12-00134.1>

866

867 Xie, S., McCoy, R. B., Klein, S. A., Cederwall, R. T., Wiscombe, W. J., Jensen, M. P., et
868 al. (2010). CLOUDS AND MORE: ARM Climate Modeling Best Estimate Data. *Bulletin of the*
869 *American Meteorological Society*, 91, 13-20. <https://doi.org/10.1175/2009BAMS2891.1>

870

871 Zhang, D., Vogelmann, A., Kollias, P., Luke, E., Yang, F., Lubin, D., & Wang, Z. (2019).

872 Comparison of Antarctic and Arctic single-layer stratiform mixed-phase cloud properties using

873 ground-based remote sensing measurements. *Journal of Geophysical Research: Atmospheres*,
874 124(17-18), 10186-10204. <https://doi.org/10.1029/2019JD030673>

875

876 Zhang, D., Wang, Z., Kollias, P., Vogelmann, A. M., Yang, K., & Luo, T. (2018). Ice particle
877 production in mid-level stratiform mixed-phase clouds observed with collocated A-Train
878 measurements. *Atmospheric Chemistry and Physics*, 18, 4317-4327. [https://doi.org/10.5194/acp-](https://doi.org/10.5194/acp-18-4317-2018)
879 18-4317-2018

880

881 Zhang, G. J., & McFarlane, N. A. (1995). Sensitivity of climate simulations to the
882 parameterization of cumulus convection in the Canadian Climate Centre general circulation
883 model. *Atmosphere-Ocean*, 33(3), 407-446. <https://doi.org/10.1080/07055900.1995.9649539>

884

885 Zhang, M., Liu, X., Diao, M., D'Alessandro, J. J., Wang, Y., Wu, C., et al (2019). Impacts of
886 representing heterogeneous distribution of cloud liquid and Ice on phase partitioning of Arctic
887 mixed-phase clouds. *Journal of Geophysical Research: Atmospheres*, 124.

888 <https://doi.org/10.1029/2019JD030502>

889

890 Zhang, Y., Xie, S., Lin, W., Klein, S. A., Zelinka, M., Ma, P.-L., et al. (2019). Evaluation of
891 clouds in version 1 of the E3SM atmosphere model with satellite simulators. *Journal of*
892 *Advances in Modeling Earth Systems*, 11. <https://doi.org/10.1029/2018MS001562>

893

894 Zhao, C., Xie, S., Klein, S. A., Protat, A., Shupe, M. D., McFarlane, S. A. et al. (2012). Toward
895 understanding of differences in current cloud retrievals of ARM ground-based
896 measurements, *Journal of Geophysical Research: Atmospheres*, 117, D10206.
897 <https://doi.org/10.1029/2011JD016792>

898

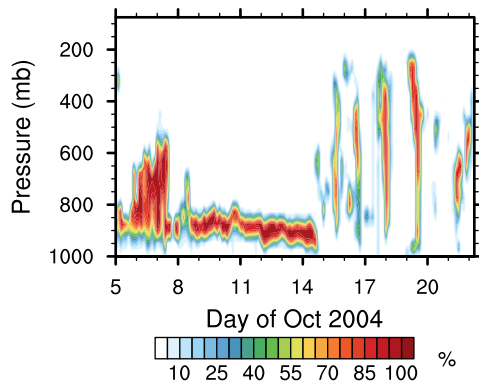
899 Zheng, X., Klein, S. A., Ma, H.-Y., Bogenschutz, P., Gettelman, A., & Larson, V.
900 E. (2016). Assessment of marine boundary layer cloud simulations in the CAM with CLUBB
901 and updated microphysics scheme based on ARM observations from the Azores. *Journal of*
902 *Geophysical Research: Atmospheres*, 121, 8472-8492, <https://doi.org/10.1002/2016JD025274>

903

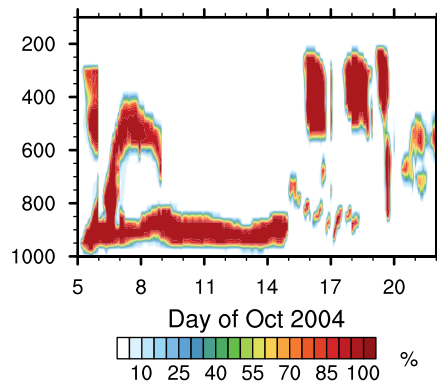
904

Figure 1.

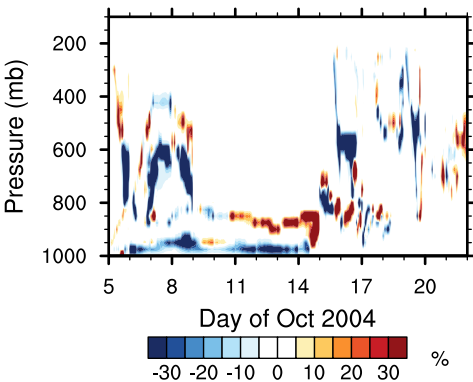
(a) ARSCL observation



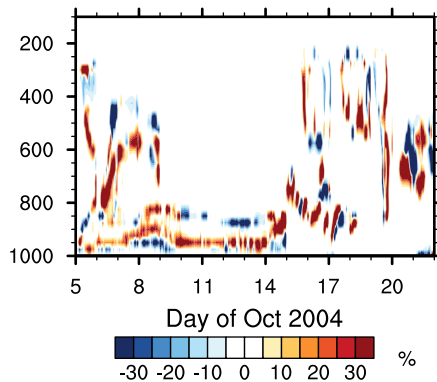
(b) CTL



(c) CLT - MEYERS



(d) CTL - UW



(e) UW - UW_MG1

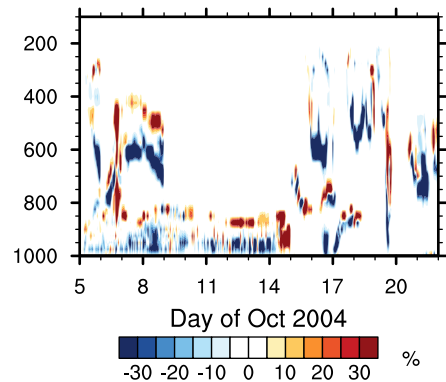


Figure 2.

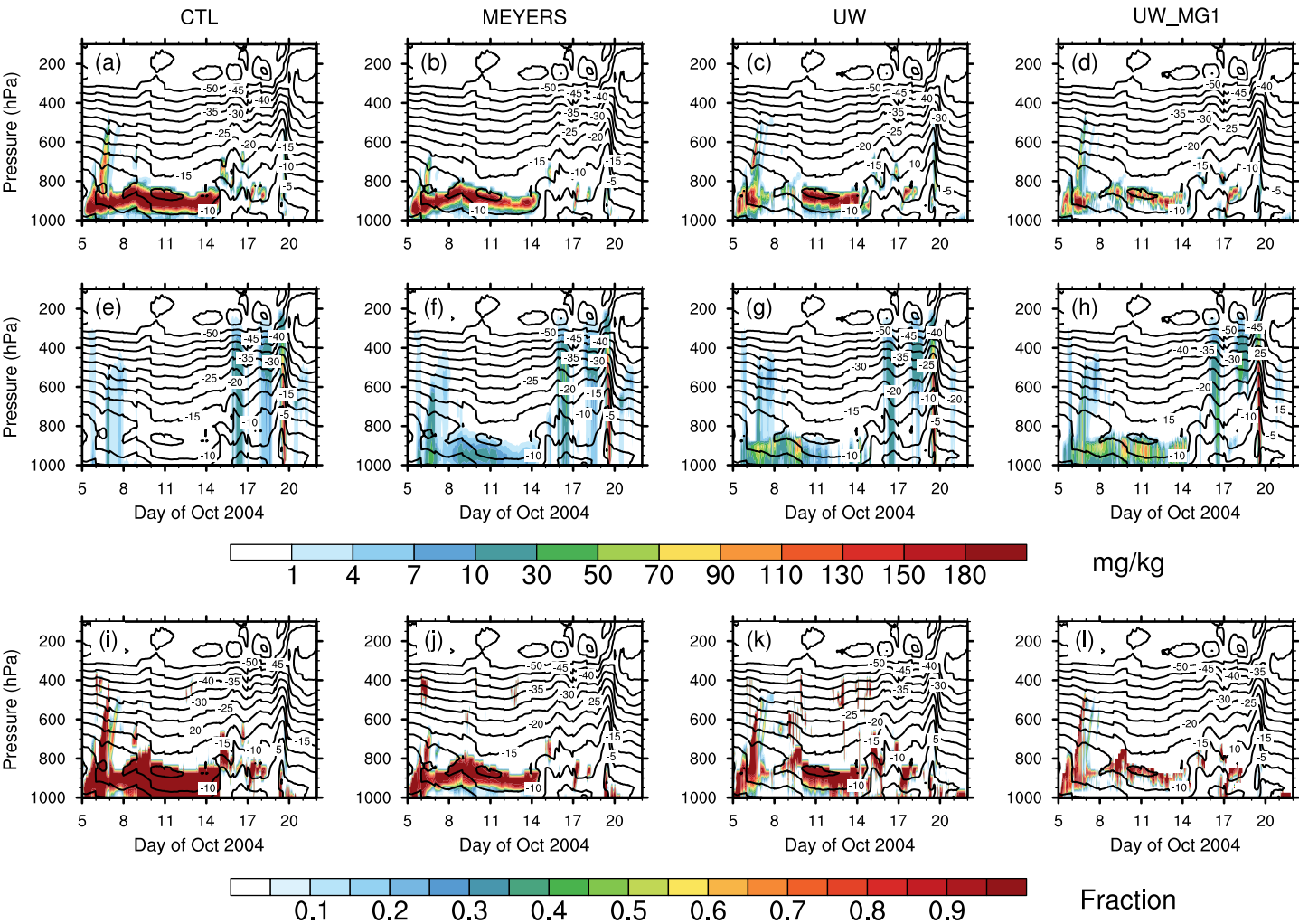
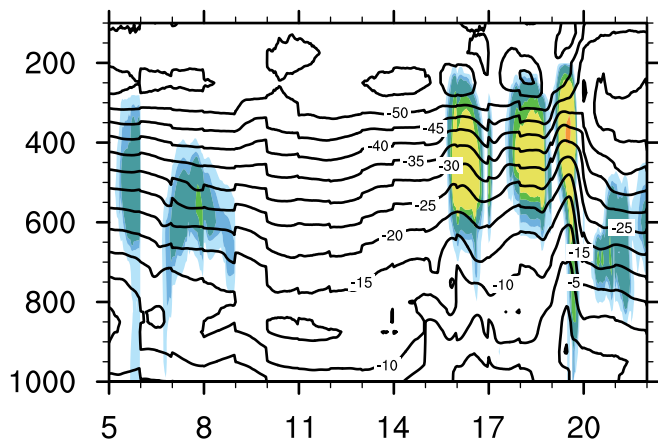
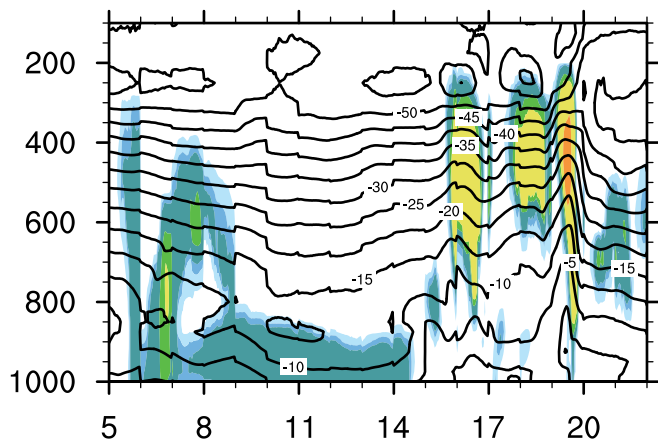


Figure 3.

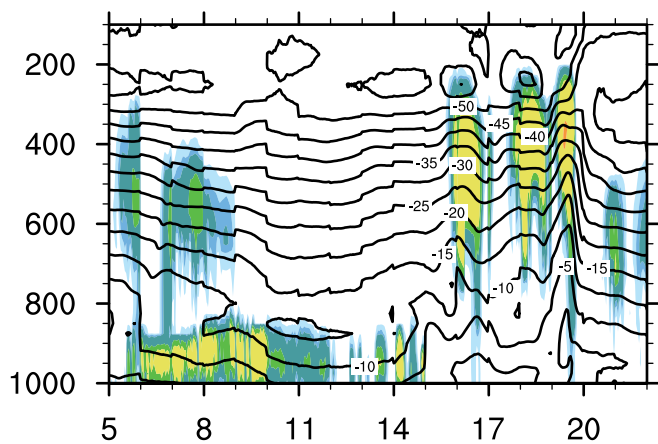
(a) CTL



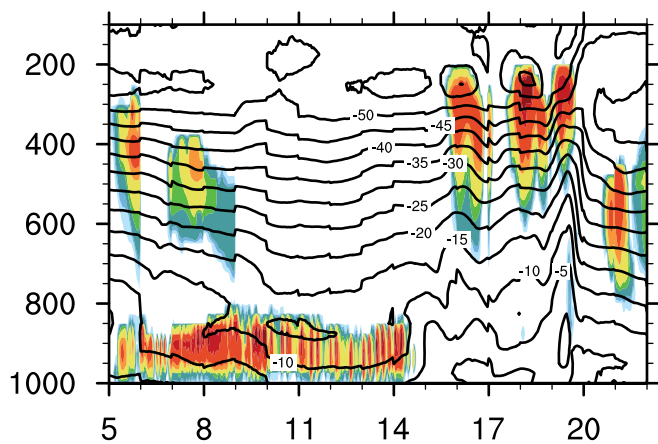
(b) MEYERS



(c) UW



(d) UW_MG1



Day of Oct 2004

Day of Oct 2004



Figure 4.

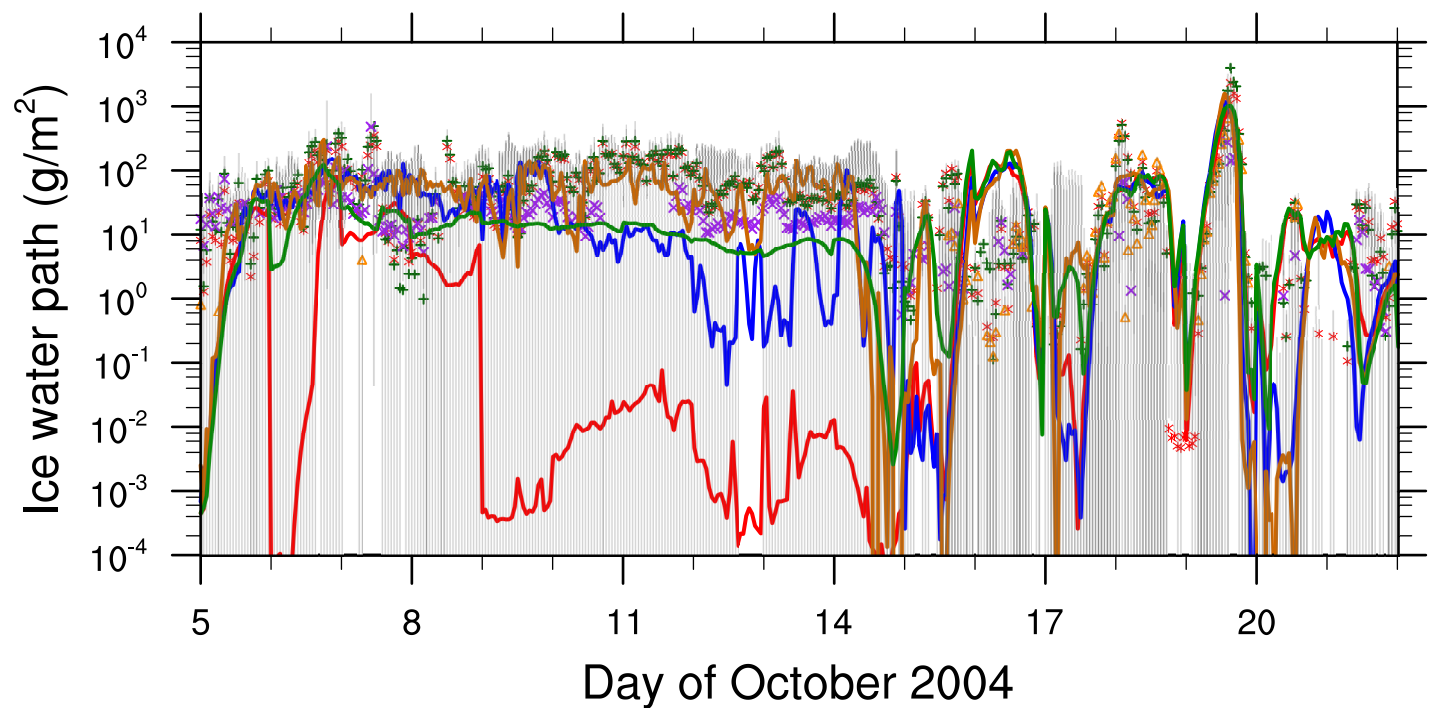
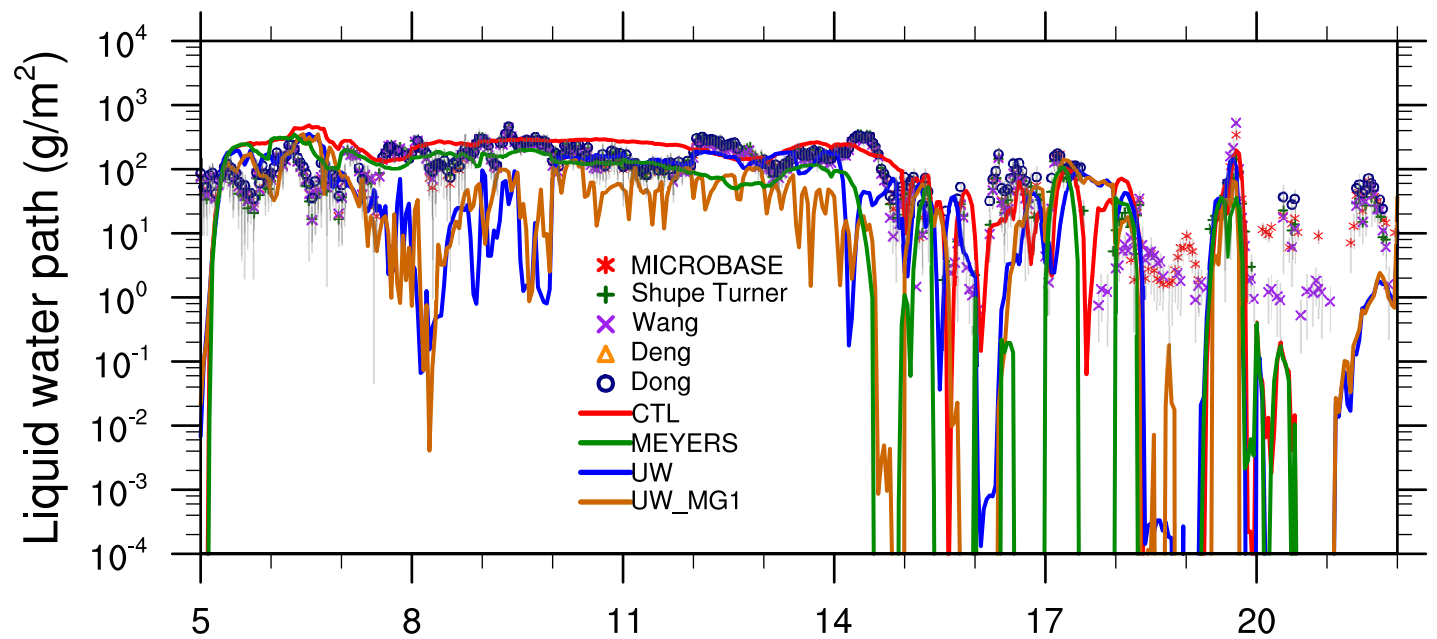


Figure 5.

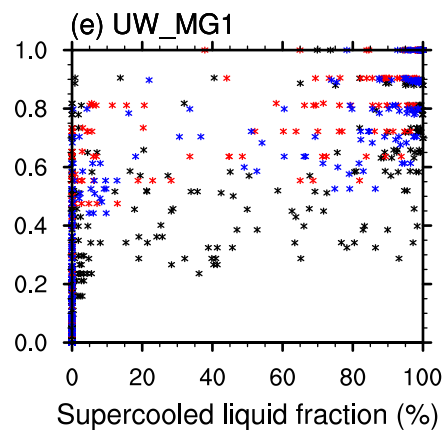
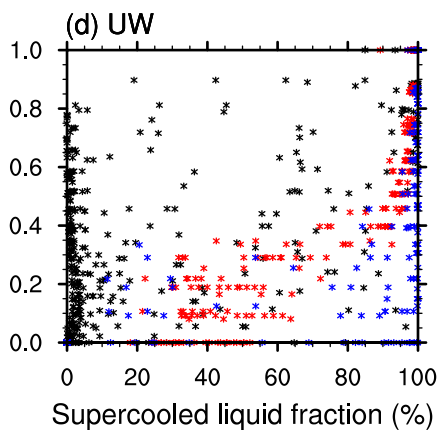
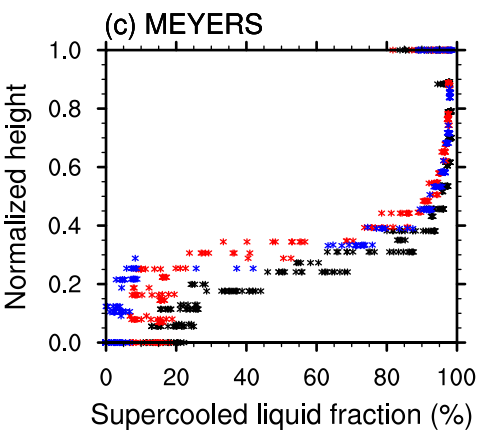
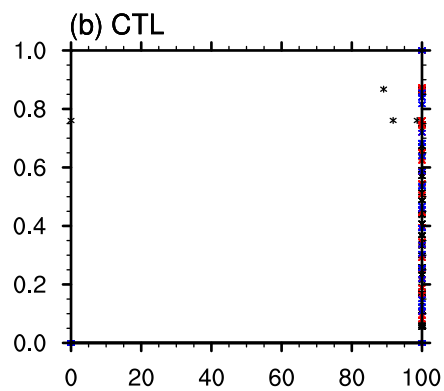
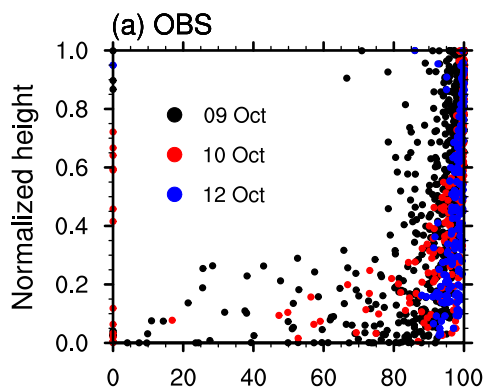
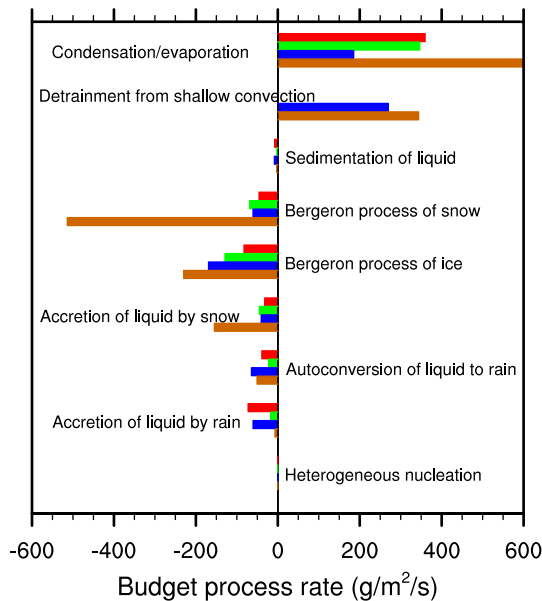
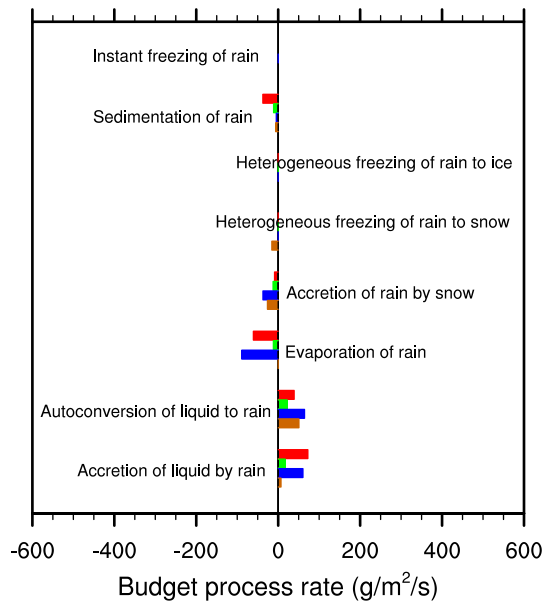


Figure 6.

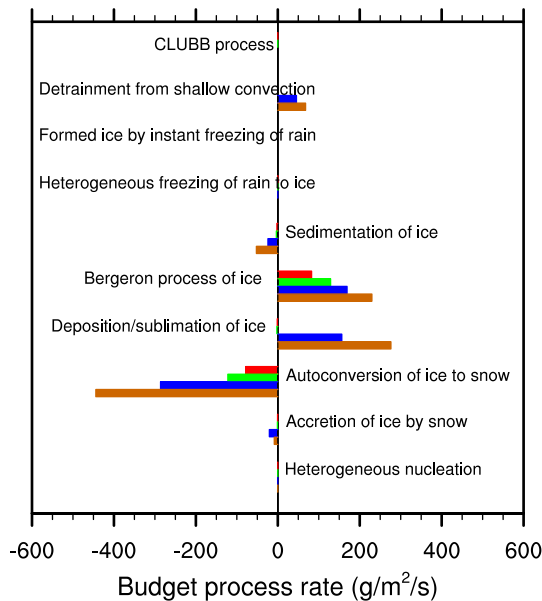
(a) LIQUID



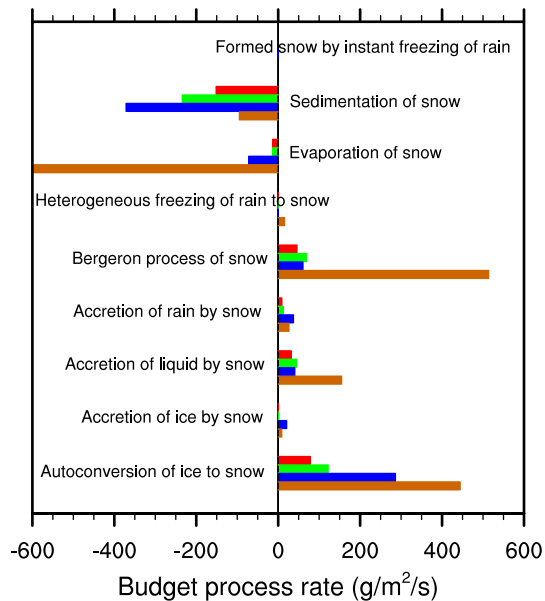
(b) RAIN



(c) ICE



(d) SNOW



CTL

MEYERS

UW

UW_MG1